

# Dependence of Lindbladian spectral statistics on the integrability of no-jump Hamiltonians and the recycling terms

Dingzu Wang,<sup>1,2</sup> Hao Zhu,<sup>3,\*</sup> Guo-Feng Zhang,<sup>3,†</sup> and Dario Poletti<sup>1,4,2,5,‡</sup>

<sup>1</sup>*Science, Mathematics and Technology Cluster, Singapore University of Technology and Design, 8 Somapah Road, 487372 Singapore*

<sup>2</sup>*Centre for Quantum Technologies, National University of Singapore 117543, Singapore*

<sup>3</sup>*School of Physics, Beihang University, 100191, Beijing, China*

<sup>4</sup>*EPD Pillar, Singapore University of Technology and Design, 8 Somapah Road, 487372 Singapore*

<sup>5</sup>*MajuLab, CNRS-UNS-NUS-NTU International Joint Research Unit, UMI 3654, Singapore*

Spectral statistics probe integrability versus chaos and have recently been extended to Markovian open quantum systems described by Lindbladians, whose quantum-trajectory unraveling decomposes the evolution into no-jump dynamics generated by an effective non-Hermitian Hamiltonian and recycling jumps. In this work, we perform spectrum-statistics diagnostics for Lindbladians and their effective non-Hermitian Hamiltonians. We show that recycling processes, symmetry constraints, and the Liouville-space structure crucially shape the spectral correlations. In particular, we identify a family of spectrally separable Lindbladians whose spectra exhibit robust Poisson statistics, despite the effective non-Hermitian Hamiltonian varying from regular to chaotic. Our work establishes a unified spectral-statistics characterization for Lindbladians and their associated effective non-Hermitian Hamiltonians, deepening our understanding of integrable and chaotic spectral properties in open many-body systems.

## I. INTRODUCTION

While quantum dynamics is often idealized as unitary, non-unitary evolution is ubiquitous because realistic systems inevitably interact with their environment. To describe such environmental effects, the theory of open quantum systems [1–3] provides a standard framework to account for dissipation and decoherence. In the Markovian (i.e., memoryless) regime, the evolution of an open quantum system is governed by the Gorini-Kossakowski-Sudarshan-Lindblad master equation [4, 5]. The generator of this master equation, the Lindbladian, underlies relaxation toward steady states and sets the characteristic dynamical timescales [1, 6, 7].

In recent years, non-Hermitian systems have attracted much attention, for instance, in the study of Lindbladian dynamics of integrable [8–13] and chaotic [14–17] open quantum systems, localization [18–22], and thermalization [23–25]. More concretely, from the quantum trajectory perspective [26–31], Lindbladian dynamics can be unraveled into stochastic trajectories consisting of random quantum jumps interspersed with no-jump segments generated by an effective non-Hermitian Hamiltonian (NHH). This conditioned description is widely used in studies of continuously monitored open systems [32–34], where postselection on no-jump trajectories makes the effective NHH directly relevant for the conditional dynamics. However, it is not obvious whether this dynamical connection carries over to the spectral correlations of the Lindbladian and those of its associated effective NHH.

The study of spectral statistics is of fundamental importance in theoretical physics, owing to its universality and its role as a robust diagnostic of integrability versus chaos [35–39]. In closed (Hermitian) systems, spectral statistics distinguish integrability from chaos, with Poisson statistics for

integrable models, characterized by uncorrelated levels, and Wigner–Dyson statistics for chaotic ones, exhibiting level repulsion as predicted by random-matrix theory (RMT) [40–42]. For open quantum systems, various extensions of spectral statistics analysis to the complex spectrum of the Lindbladian have been proposed [15, 43–47]. In this context, complex spectral statistics have become a broadly useful probe of universal behavior in open and non-Hermitian many-body systems [48–60]. This raises the concrete question of whether the spectral statistics of the Lindbladian reflects that of its no-jump generator and, if not, what role is played by the quantum-jump (recycling) term.

In this work, we explore this question by characterizing the spectral statistics of Lindbladians and their no-jump effective non-Hermitian Hamiltonians within a unified set of complex spectrum diagnostics. We map out the four possible combinations of integrability and chaos for the two generators and demonstrate each in paradigmatic dissipative spin chains, highlighting how the recycling contribution and the coherent Hamiltonian structure can reshape the spectral correlations. We then focus on a class of Lindbladians describing  $U(1)$ -symmetric systems with local damping that we refer to as *spectrally separable*, i.e., for which the spectrum admits an exact construction from the associated no-jump effective NHH. Within this family, the Lindbladian exhibits robust Poisson statistics in the complex spectrum despite the associated no-jump non-Hermitian Hamiltonian can vary between chaotic and Poisson-like behavior. In the special case of spatially uniform damping, we uncover an extra phenomenology in which the level statistics can resemble real-spectrum Poissonian behavior, even though the Lindbladian itself has a genuinely complex spectrum.

The remainder of this paper is organized as follows. In Sec. II, we introduce the Lindbladian and the associated no-jump effective non-Hermitian Hamiltonian, formulate the ladder representation used for symmetry resolution, and summarize the spectral diagnostics employed throughout. In Sec. III, we present the main correspondence scenarios by analyzing

\* Corresponding author: [zhuha06590@buaa.edu.cn](mailto:zhuha06590@buaa.edu.cn)

† Corresponding author: [gf1978zhang@buaa.edu.cn](mailto:gf1978zhang@buaa.edu.cn)

‡ Corresponding author: [dario.poletti@sutd.edu.sg](mailto:dario.poletti@sutd.edu.sg)

paradigmatic dissipative spin chains, and demonstrate how correspondence or breakdown can arise under different dissipative channels. In Sec. IV, we identify a broad class of systems in which the Lindbladian presents Poissonian statistics independently of the statistics of the non-Hermitian Hamiltonian. Finally, Sec. V provides a summary and an outlook.

## II. SPECTRAL ANALYSIS SCHEME

In this section, we first introduce the Lindbladian dynamics and its no-jump effective non-Hermitian Hamiltonian, and then present the ladder representation and spectral diagnostics used throughout this work.

### A. Lindbladian and no-jump effective Hamiltonian

We consider Markovian open quantum systems whose density matrix evolves according to the Gorini-Kossakowski-Sudarshan-Lindblad master equation [1, 3–5], i.e.,  $\dot{\rho} = \mathcal{L}[\rho]$ , where the Lindbladian superoperator  $\mathcal{L}$  is given by

$$\mathcal{L}[\rho] = -i[H, \rho] + \sum_i (L_i \rho L_i^\dagger - \frac{1}{2}\{L_i^\dagger L_i, \rho\}), \quad (1)$$

with  $H$  the system Hamiltonian, and  $\{L_i\}$  the jump operators modeling the system-environment coupling, and we set  $\hbar = 1$  throughout.

It is often convenient to rewrite the Lindbladian in a form that separates the conditional no-jump evolution from the recycling processes,

$$\mathcal{L}[\rho] = -i(H_{\text{eff}}\rho - \rho H_{\text{eff}}^\dagger) + \sum_i L_i \rho L_i^\dagger, \quad (2)$$

where the no-jump effective non-Hermitian Hamiltonian is defined as

$$H_{\text{eff}} = H - \frac{i}{2} \sum_i L_i^\dagger L_i. \quad (3)$$

Within the quantum-trajectory picture, the non-Hermitian evolution generated by  $H_{\text{eff}}$  describes the conditioned dynamics between quantum jumps, while the recycling term  $\sum_i L_i \rho L_i^\dagger$  accounts for stochastic jump events. Ensemble averaging over such trajectories reproduces the dynamics of the density matrix.

### B. Ladder representation and symmetries

To diagnose integrability versus chaos from spectral statistics, it is essential to resolve all relevant symmetries. For Lindbladians, this task is more subtle than for isolated Hamiltonians, since the generator acts in a doubled Hilbert space and symmetries acting on ket and bra degrees of freedom can be

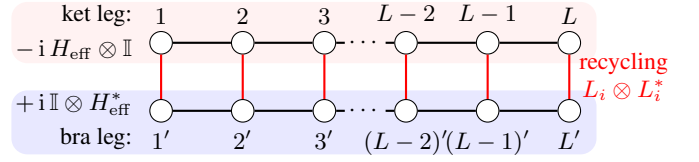


FIG. 1. Depiction of Ladder representation of the Lindbladian  $\mathbb{L}$ . The upper (lower) leg corresponds to the ket (bra) Hilbert space. The no-jump part acts independently on the two legs as  $-i H_{\text{eff}} \otimes \mathbb{I}$  and  $+i \mathbb{I} \otimes H_{\text{eff}}^*$ , while the recycling term generates inter-leg couplings on each rung,  $L_i \otimes L_i^*$ . Here  $i$  labels the site on the ket leg corresponding to site  $i'$  on the bra leg.

intertwined. Hence, we interpret the Lindbladian superoperator as a non-Hermitian operator that acts on a *ladder* structure, which provides a physically transparent organization of the doubled Hilbert space, and allows symmetry analysis to be carried out in close analogy with ordinary Hamiltonian systems (see Fig. 1).

This ladder formulation corresponds to working in Liouville space, where the density matrix is vectorized as  $|\rho\rangle\rangle = \sum_{m,n} \rho_{mn} |m, n\rangle\rangle$ , and the master equation takes the form  $(d/dt)|\rho\rangle\rangle = \mathbb{L}|\rho\rangle\rangle$  (see, e.g., [7]). In this formulation, the Lindbladian  $\mathbb{L}$  acts as a linear operator on Liouville space, i.e., a doubled Hilbert space spanned by the ket and bra degrees of freedom, and takes the explicit form

$$\mathbb{L} = -i(H_{\text{eff}} \otimes \mathbb{I} - \mathbb{I} \otimes H_{\text{eff}}^*) + \sum_i L_i \otimes L_i^*. \quad (4)$$

In this vectorized representation, the ladder structure is naturally revealed, since the no-jump evolution generated by  $H_{\text{eff}}$  acts independently on the two legs, while the recycling term  $L_i \rho L_i^\dagger$  gives rise to inter-leg couplings. In the following, we discuss how  $U(1)$  and spatial symmetries are manifest in Liouville space, and how they can be exploited for symmetry considerations.

When the Lindbladian satisfies  $[\mathbb{L}, \mathcal{M}_p] = 0$ , with  $\mathcal{M}_p = \sum_{i=1}^L \sigma_i^z + \sum_{i=1}^{L'} \sigma_i^z$ , the generator  $\mathbb{L}$  admits a global  $U(1)$  symmetry in Liouville space. The sum runs over  $2L$  sites, reflecting the ladder representation in Liouville space, such that  $\mathcal{M}_p$  is given by the sum of the magnetizations associated with each leg. In addition to this total magnetization symmetry, the ladder representation also manifests clearly a second  $U(1)$  symmetry associated with the magnetization difference between the two legs. For certain Lindbladians, this quantity is conserved, generated by  $\mathcal{M}_d = \sum_{i=1}^L \sigma_i^z - \sum_{i=1}^{L'} \sigma_i^z$ , such that  $[\mathbb{L}, \mathcal{M}_d] = 0$ . The generators  $\mathcal{M}_p$  and  $\mathcal{M}_d$  provide a natural Liouville-space organization of conserved charges and connect to the notions of strong and weak symmetries in open quantum systems [61]. When both symmetries are present, the Lindbladian block-diagonalizes into joint  $(m_p, m_d)$  sectors. The allowed values are constrained by  $m_p = m_{\text{ket}} + m_{\text{bra}}$  and  $m_d = m_{\text{ket}} - m_{\text{bra}}$ , where  $m_{\text{ket}}$  and  $m_{\text{bra}}$  denote the magnetizations on the ket and bra legs, respectively. As a consequence,  $m_p$  and  $m_d$  must either both be even or odd.

We now turn to spatial symmetries of the Lindbladian. For

systems with spatially uniform Hamiltonians and homogeneous dissipation, the ladder representation makes the spatial reflection symmetry  $P_x$  along the chain direction manifest in Liouville space, allowing it to be resolved in the same way as an  $x$ -direction spatial inversion in lattice systems. In this form,  $P_x$  can also be combined naturally with the  $U(1)$  symmetries discussed above.

By contrast, reflection along the  $y$ -direction of the ladder, denoted as  $P_y$ , does not generically commute with the Lindbladian. Nevertheless, it plays a distinguished role in the ladder representation, as it allows one to choose a particularly convenient basis in the Liouville space. Specifically, one can work in a basis formed by states that are symmetric and anti-symmetric under the ladder reflection  $P_y$ ,

$$\begin{aligned} |\phi_{mn}^{\text{sym}}\rangle &= \frac{1}{\sqrt{2}}(|m, n\rangle + P_y|m, n\rangle), \\ |\phi_{mn}^{\text{asym}}\rangle &= \frac{i}{\sqrt{2}}(|m, n\rangle - P_y|m, n\rangle), \end{aligned} \quad (5)$$

for  $m \neq n$ , where  $|m, n\rangle$  denotes the Liouville-space basis introduced above through vectorization, and  $P_y|m, n\rangle = |n, m\rangle$  acts by exchanging the two legs of the ladder. For  $m = n$ ,  $|\phi_{mm}^{\text{sym}}\rangle$  reduces to  $|m, m\rangle$ . In this  $P_y$ -(anti)symmetric basis, the Liouville-space vector  $|\rho\rangle$  is parametrized by purely real coefficients, corresponding to the real and imaginary parts of the density matrix elements, as a direct consequence of its Hermiticity. Since the Lindblad master equation preserves Hermiticity, this real structure is invariant under time evolution, implying that the Lindbladian is represented by a purely real matrix in this basis.

An equivalent way to express this structure is in terms of an antiunitary symmetry of the Lindbladian. The antiunitary operator  $\mathcal{T}$  is defined by  $\mathcal{T}|A\rangle = |A^\dagger\rangle$ , which in the ladder representation corresponds to  $\mathcal{T} = P_y K$ , where  $K$  denotes complex conjugation. Hermiticity preservation implies  $[e^{t\mathcal{L}}(\rho)]^\dagger = e^{t\mathcal{L}}(\rho^\dagger)$  for any density operator  $\rho$  [62]. In vectorized form, this implies  $\mathcal{T}e^{t\mathbb{L}}|\rho\rangle = [e^{t\mathcal{L}}(\rho)]^\dagger = |e^{t\mathcal{L}}(\rho^\dagger)\rangle = e^{t\mathbb{L}}\mathcal{T}|\rho\rangle$  for all  $|\rho\rangle$ , and hence

$$\mathcal{T}e^{t\mathbb{L}}\mathcal{T}^{-1} = e^{t\mathbb{L}}, \quad \mathcal{T}\mathbb{L}\mathcal{T}^{-1} = \mathbb{L}. \quad (6)$$

Resolving this time-reversal symmetry [59] in the  $P_y$ -(anti)symmetric basis, leads directly to a purely real matrix representation of the Lindbladian, improving numerical efficiency.

### C. Spectral diagnostics

Spectral signatures of integrability and chaos in open and non-Hermitian systems require diagnostics beyond the standard Hermitian level statistics. We therefore use a set of complementary indicators that have been developed recently for complex spectra, and apply them consistently to both the Lindbladian  $\mathbb{L}$  and its no-jump effective Hamiltonian  $H_{\text{eff}}$ .

As a basic probe of spectral statistics, we use the nearest-neighbor level-spacing distribution of the complex eigenvalues of  $\mathbb{L}$  and  $H_{\text{eff}}$ . The distribution  $P(s)$  of spacings

$s_n = \min_{n \neq n'} |E_n - E_{n'}|$  in the complex plane shows different behavior depending on whether the system is integrable or chaotic. In integrable regimes, where the eigenvalues are effectively uncorrelated in the complex plane,  $P(s)$  is well described by the two-dimensional (2D) Poisson distribution [43, 44]

$$P_{\text{Poi}}(s) = \frac{\pi}{2} s e^{-\pi s^2/4}. \quad (7)$$

In the fully chaotic regime, the spacings are expected to follow the Ginibre ensemble of complex non-Hermitian Gaussian random matrices (GinUE), with the Ginibre distribution  $P_{\text{Gin}}(s)$  given by [39, 46, 63, 64]

$$P_{\text{Gin}}(s) = c \lim_{M \rightarrow \infty} \left( \prod_{m=1}^{M-1} e_m(s^2) e^{-s^2} \right) \sum_{m=1}^{M-1} \frac{2s^{2m+1}}{m! e_m(s^2)} \quad (8)$$

with  $e_m(s^2) = \sum_{l=0}^m s^{2l}/l!$  and  $c \simeq 1.1429$ . In practice, we unfold the complex spectrum by rescaling distances with the local spectral density, so that the mean spacing is unity [44].

Another useful spectral diagnostic, which does not require spectral unfolding, is the complex spacing ratio (CSR), as introduced in Ref. [45]

$$z_n = \frac{E_n^{\text{NN}} - E_n}{E_n^{\text{NNN}} - E_n}, \quad (9)$$

where  $E_n^{\text{NN}}$  and  $E_n^{\text{NNN}}$  denote, respectively, the nearest- and next-nearest-neighbors of  $E_n$  with respect to the distance in the complex plane. By construction, all complex spacing ratios lie inside the unit disk and encode both radial and angular information about the complex spectrum. For integrable spectra, the complex spacing ratios are expected to be approximately uniform in the unit disk. In contrast, for chaotic spectra the CSR distribution shows a reduced probability density at small radii and a nonuniform angular profile, reflecting level repulsion in the complex plane.

In addition to complex eigenvalues, we also consider the singular-value statistics of  $\mathbb{L}$  and  $H_{\text{eff}}$ , following Ref. [47], which enables the use of real-spectrum chaos diagnostics familiar from Hermitian systems. Given a generic non-Hermitian matrix  $A$  (here  $A = \mathbb{L}$  or  $H_{\text{eff}}$ ), we obtain its singular values from the singular-value decomposition  $A = U S V^\dagger$ , where  $S = \text{diag}(s_1, \dots, s_N)$  collects the singular values  $s_n$ . Equivalently, the same set  $\{s_n\}$  can be obtained via the Hermitization method [65] as the positive square roots of the eigenvalues of the Hermitian matrices  $M^\dagger M$  or  $M M^\dagger$ . In contrast to eigenvalues, singular values are always real and nonnegative even for non-Hermitian matrices. We characterize spectral statistics using the singular-value spacing ratio for the ordered set  $\{s_n\}$ ,

$$r_n = \min \left( \frac{s_{n+1} - s_n}{s_n - s_{n-1}}, \frac{s_n - s_{n-1}}{s_{n+1} - s_n} \right), \quad (10)$$

in analogy with spacing ratios of real eigenvalues in Hermitian random-matrix theory [66, 67]. In integrable regimes,

the ratios are expected to follow Poisson statistics, with an average value  $\langle r \rangle \simeq 0.3863$ . For chaotic singular spectra, the spacing-ratio distribution coincides with that of the corresponding Hermitian Gaussian random-matrix ensemble in the appropriate symmetry class, with the associated class-dependent average value  $\langle r \rangle$  summarized in Ref [47]. In this work, we analyze the traceless operators  $\mathbb{L} - (\text{tr}\mathbb{L}/\text{tr}\mathbb{I})\mathbb{I}$  and  $H_{\text{eff}} - (\text{tr}H_{\text{eff}}/\text{tr}\mathbb{I})\mathbb{I}$ .

We note that, while singular-value statistics provide convenient Hermitian-like diagnostics for non-Hermitian matrices, recent works have pointed out that SVD-based spectral correlations may disagree with eigenvalue-based complex-spectrum diagnostics in certain settings [68, 69]. Accordingly, throughout this work we use singular-value statistics as a complementary probe, and rely on eigenvalue-based diagnostics ( $P(s)$  and CSR) to establish the integrable/chaotic classification.

### III. SPECTRAL CORRESPONDENCE AND ITS BREAKDOWN

In this section, we perform a systematic comparison of the spectral statistics of Lindbladians  $\mathbb{L}$  and their associated no-jump effective Hamiltonians  $H_{\text{eff}}$ , focusing on when correspondence between the two generators is preserved or breaks down. We begin with the chaotic regime exhibiting spectral correspondence and then turn to the integrable regime to explore whether integrable spectral statistics of  $H_{\text{eff}}$  are inherited by the full Lindbladian  $\mathbb{L}$ . The complementary scenario, in which the full Lindbladian exhibits Poissonian spectral statistics due to spectral separability, is deferred to the next section.

#### A. Correspondence in the chaotic regime

We first illustrate a regime where the spectral diagnostics of the Lindbladian  $\mathbb{L}$  and the no-jump non-Hermitian Hamiltonian  $H_{\text{eff}}$  are consistent and both indicate quantum chaos. As a representative realization, we consider a dissipative transverse-field Ising (TFI) chain with open boundary conditions,

$$H_{\text{TFI}} = J \sum_{i=1}^{L-1} \sigma_i^z \sigma_{i+1}^z + h \sum_{i=1}^L \sigma_i^x, \quad (11)$$

where  $L$  is the number of spins, and  $\sigma_i^{x,z}$  denote Pauli operators acting on site  $i$ . The parameters  $J$  and  $h$  set the nearest-neighbor coupling strength and the transverse field, respectively. This TFI model is integrable and can be mapped to free fermions via a Jordan–Wigner transformation. In the thermodynamic limit, it exhibits a quantum phase transition at  $h = J$ . Dissipation is introduced via local damping jump operators,

$$L_i = \sqrt{\gamma_i} \sigma_i^-, \quad (12)$$

where  $\gamma_i$  denotes the local dissipation rate. In this section, we consider uniform dissipation and set  $\gamma_i = \gamma$  for all sites, with

$\gamma$  controlling the overall dissipation strength. For this choice of Hamiltonian and jump operators, both  $\mathbb{L}$  (in the ladder representation) and  $H_{\text{eff}}$  respect the spatial reflection symmetry  $P_x$ . In the following, we restrict the spectral analysis to the even- $P_x$  sector for both generators. We compute the complex spectra by exact diagonalization for system size up to  $L = 9$  for  $\mathbb{L}$  and  $L = 18$  for  $H_{\text{eff}}$ . In the largest case studied, the Hilbert-space dimension is 131,328, and we set  $h = 1.05J$  and  $\hbar\gamma = J$ .

We first analyze the nearest-neighbor level-spacing distribution  $P(s)$  of the complex eigenvalues for  $H_{\text{eff}}$  and  $\mathbb{L}$ , shown in Figs. 2(a) and 2(b), respectively. Here,  $P(s)$  closely matches the GinUE distribution Eq. (8) (the blue curve), indicating quantum chaotic spectral correlations for both generators. From the correspondence viewpoint, the damping channel contributes to the non-Hermitian terms in  $H_{\text{eff}}$  and recycling processes in  $\mathbb{L}$ , which break the free-fermion integrable structure and drive both spectra toward GinUE statistics.

For  $H_{\text{eff}}$ , we further find that  $P(s)$  is well captured by the two-dimensional Coulomb-gas description [44, 70] at inverse temperature  $\beta = 1.6$  (with  $\beta = 0$  and  $\beta = 2$  corresponding to the 2D Poisson and GinUE limits, respectively). As shown in Fig. 2(a),  $\beta = 1.6$  (black dashed curve) provides an excellent match to the numerical distribution, where the Coulomb-gas reference curve is obtained by Monte Carlo sampling of the joint distribution [44, 71]. This intermediate form is expected to flow toward the GinUE limit with increasing Hilbert-space dimension.

Additionally, we examine the distribution of the complex spacing ratios (CSR)  $z_n$  for  $H_{\text{eff}}$  and  $\mathbb{L}$ , shown in Figs. 2(c) and 2(d), respectively. For both generators, the CSR distribution shows a pronounced suppression near the origin and a clearly anisotropic angular profile, consistent with level repulsion in the complex plane [45]. These features are characteristic of chaotic spectral correlations, in contrast to the uniform CSR expected for integrable spectra. The CSR therefore provides a consistent chaos diagnosis for both  $H_{\text{eff}}$  and  $\mathbb{L}$ , in agreement with the level-spacing distribution.

While  $P(s)$  and the CSR already establish chaos for both generators, we next turn to singular-value statistics to probe whether this chaos–chaos correspondence persists at the level of symmetry (universality) classes. Specifically, we compute the singular-value spacing ratios  $r_n$  and the mean  $\langle r \rangle$  for  $H_{\text{eff}}$  and  $\mathbb{L}$ , as depicted in Figs. 2(e) and 2(f). Fig. 2(e) shows that the singular-value statistics of  $\mathbb{L}$  belong to class AI, whereas those of  $H_{\text{eff}}$  are consistent with class  $\text{BDI}^\dagger$  [47]. This assignment is also corroborated by the mean ratio  $\langle r \rangle$  in Fig. 2(f), shown as a function of the dissipation strength  $\gamma$ . We find that  $\langle r \rangle$  rapidly approaches class values  $\langle r \rangle_{\text{AI}} = 0.5358$  for  $\mathbb{L}$  and  $\langle r \rangle_{\text{BDI}^\dagger} = 0.4210$  for  $H_{\text{eff}}$  [72], and remains stable across the explored range of  $\gamma$ . This is expected since  $\mathbb{L}$  admits an antiunitary time-reversal symmetry (see Sec. II B), placing its singular-value statistics in class AI. For  $H_{\text{eff}}$  considered here, the no-jump Hamiltonian respects time-reversal symmetry<sup>†</sup>

$$H_{\text{eff}}^T = H_{\text{eff}}. \quad (13)$$

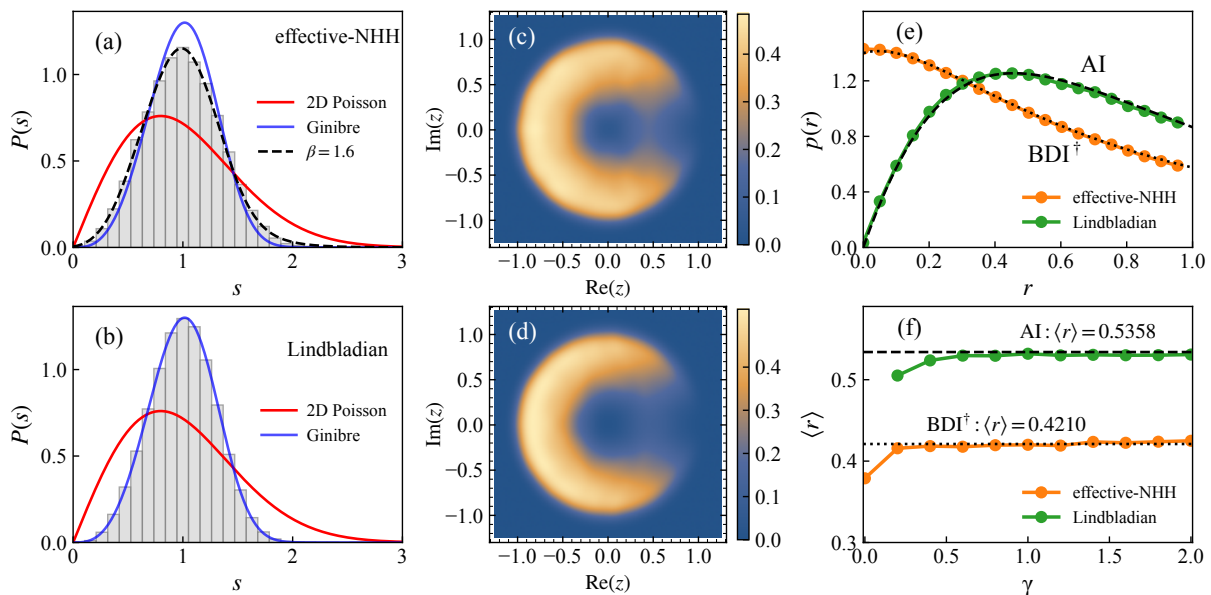


FIG. 2. Spectral diagnostics for the no-jump effective non-Hermitian Hamiltonian  $H_{\text{eff}}$  and the Lindbladian  $\mathbb{L}$  in the dissipative transverse-field Ising chain with local damping. (a), (b) Nearest-neighbor level-spacing distribution  $P(s)$  of the complex spectrum for (a)  $H_{\text{eff}}$  and (b)  $\mathbb{L}$ , compared with the two-dimensional (2D) Poisson distribution (red) and the Ginibre ensemble (blue); the dashed curve in (a) shows a Coulomb-gas reference at inverse temperature  $\beta = 1.6$ . (c), (d) Distribution of complex spacing ratios (CSR)  $z_n$  for (c)  $H_{\text{eff}}$  and (d)  $\mathbb{L}$ . (e) Singular-value spacing-ratio distribution  $p(r)$ ; the black dashed curves are the analytical results for small non-Hermitian random matrices in classes AI and  $\text{BDI}^\dagger$ . (f) Mean ratio  $\langle r \rangle$  versus dissipation strength  $\gamma$ , with dashed (AI) and dotted ( $\text{BDI}^\dagger$ ) lines. For the singular-value statistics in (e), (f), we discard 10% of singular values at both spectral edges to suppress finite-size edge effects. (a)–(e) are computed at  $\hbar\gamma = J$ .

Moreover,  $iH_{\text{eff}}$  has a particle-hole symmetry<sup>†</sup>

$$\left( \prod_{i=1}^L \sigma_i^x \right) (iH_{\text{eff}})^* \left( \prod_{i=1}^L \sigma_i^x \right)^{-1} = -iH_{\text{eff}}. \quad (14)$$

The corresponding chiral symmetry follows from the combination of these two symmetries, placing the singular-value statistics of  $H_{\text{eff}}$  in class  $\text{BDI}^\dagger$  [47]. This demonstrates that even when both generators are chaotic spectral correlations, their singular-value statistics can fall into different symmetry classes, revealing a finer-grained mismatch between  $\mathbb{L}$  and  $H_{\text{eff}}$ .

## B. Inheritance of integrable spectral statistics

We now turn to study whether integrable spectral statistics of the no-jump non-Hermitian Hamiltonian  $H_{\text{eff}}$  can be inherited by the full Lindbladian  $\mathbb{L}$ . Specifically, we consider an interacting XXZ spin-1/2 chain and a non-interacting TFI chain, where integrability arises from Bethe-ansatz and free-fermionic structures respectively, both coupled to dephasing noise. This comparison goes beyond the single Hamiltonian–dissipation setting considered above and allows us to examine how different integrable structures in  $H_{\text{eff}}$  influence the spectral statistics of the full Lindbladian.

We first study an XXZ spin-1/2 chain of length  $L$  with open

boundary conditions,

$$H_{\text{XXZ}} = J \sum_{i=1}^{L-1} (\sigma_i^x \sigma_{i+1}^x + \sigma_i^y \sigma_{i+1}^y + \Delta \sigma_i^z \sigma_{i+1}^z), \quad (15)$$

where  $J$  sets the nearest-neighbor exchange energy scale, and  $\Delta$  controls the Ising anisotropy along the  $z$  axis. The XXZ chain is Bethe-ansatz solvable and thus integrable. Dissipation is introduced via local dephasing jump operators

$$L_i = \sqrt{\gamma} \sigma_i^z, \quad (16)$$

with  $\gamma$  controlling the uniform dephasing strength in Eq. (1).

For this choice of Hamiltonian and dephasing jumps, both  $H_{\text{eff}}$  and  $\mathbb{L}$  exhibit  $U(1)$  conservation of total  $z$ -magnetization, spatial reflection  $P_x$ , and a global spin-inversion  $\mathbb{Z}_2$  symmetry. In addition,  $\mathbb{L}$  conserves the magnetization imbalance between the ket and bra legs, generated by the magnetization difference operator  $\mathcal{M}_d$  (see Sec. II B). Working in joint  $(m_p, m_d)$  sectors, the  $\mathbb{Z}_2$  spin inversion maps  $(m_p, m_d) \mapsto (-m_p, -m_d)$ , and thus acts within a sector only when the selected sector is self-mapped. In the following, we set  $\Delta = 1.05J$ , and  $\hbar\gamma = J$ , and perform exact diagonalization for a chain of length  $L = 11$  for  $\mathbb{L}$ . We focus on the even- $P_x$  sector of  $\mathbb{L}$  within the fixed  $(m_p, m_d) = (2, 0)$  block, where the global spin-inversion symmetry does not act internally.

In this dephasing setting, the effective NHH,  $H_{\text{eff}}$ , reduces to the isolated XXZ Hamiltonian up to an overall constant imaginary shift, and therefore retains integrable spectral

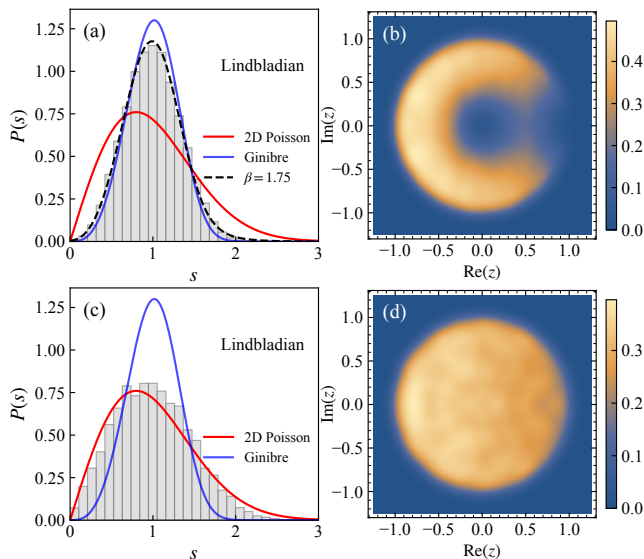


FIG. 3. Spectral diagnostics for Lindbladians  $\mathbb{L}$  in dephasing spin chains at  $\hbar\gamma = J$ . Upper row: dephasing  $XXZ$  chain; (a) nearest-neighbor level-spacing distribution  $P(s)$ , compared with the 2D Poisson statistics (red) and Ginibre ensemble (blue), with a Coulomb-gas reference (black dashed) at  $\beta = 1.75$ ; (b) corresponding complex spacing ratio (CSR) distribution. Lower row: dephasing transverse-field Ising chain; (c) level spacing distribution  $P(s)$ ; (d) corresponding CSR distribution.

statistics. For the Lindbladian, however, the dephasing channel generates Ising-type rung interactions in the ladder picture, i.e.,  $ZZ$ -type couplings between the ket and bra legs. In the interacting  $XXZ$  case, these rung interactions act as nontrivial couplings and lead to chaotic spectral correlations. Specifically, Fig. 3(a) shows that  $P(s)$  for  $\mathbb{L}$  closely follows the GinUE statistics, with the dashed curve giving a Coulomb-gas reference at inverse temperature  $\beta = 1.75$ . This is further supported by Fig. 3(b), where the CSR distribution displays a strongly nonuniform bulk pattern within the unit disk. These results provide a structural route to the integrable-chaotic scenario: for dephasing jumps, the non-Hermitian part of  $H_{\text{eff}}$  is only an overall imaginary shift, while  $\mathbb{L}$  is chaotic due to the recycling terms.

We now turn to the dephasing channel acting on a free-fermionic integrable Hamiltonian, namely the TFI chain introduced in Eq. (11). For this choice of Hamiltonian and jump operators, both  $\mathbb{L}$  and  $H_{\text{eff}}$  respect the spatial reflection symmetry  $P_x$  and the spin-inversion  $\mathbb{Z}_2$  symmetry. In the following calculations, we set  $\hbar = 1.05J$ , and  $\hbar\gamma = J$  for a chain of length  $L = 9$  for  $\mathbb{L}$  and focus on the sector with even- $\mathbb{Z}_2$  parity and even- $P_x$  parity.

In this dephasing setting,  $H_{\text{eff}}$  also remains integrable since its spectrum differs from that of the isolated TFI Hamiltonian only by an overall imaginary shift. For the full Lindbladian, the lower panels of Fig. 3 show that the spectral diagnostics are consistent with integrable statistics. Specifically, the complex spacing distribution  $P(s)$  follows the 2D Poisson form [Fig. 3(c)], and the CSR distribution is close to uniform within

the unit disk [Fig. 3(d)]. By contrast to the interacting  $XXZ$  chain, the dephasing-induced rung interactions in the Lindbladian do not induce chaotic correlations in this open non-interacting TFI model.

These two dephasing settings constitute a controlled structural comparison under an identical dissipative channel. While the interacting  $XXZ$  chain exhibits an integrable-chaotic scenario, with an integrable no-jump  $H_{\text{eff}}$  but chaotic spectral statistics of the full Lindbladian  $\mathbb{L}$ , the free-fermionic transverse-field Ising chain instead realizes an integrable-integrable scenario, with both  $H_{\text{eff}}$  and  $\mathbb{L}$  retaining integrable spectral statistics. These results demonstrate that, for the dephasing channel, the inheritance of integrable spectral statistics by the Lindbladian depends sensitively on the underlying integrable structure of the coherent Hamiltonian, and is not determined by the dissipative channel alone.

#### IV. POISSONIAN LINDBLADIAN SPECTRA FROM STRUCTURAL CONSTRAINTS

In this section, we address the complementary scenario announced above: a chaotic no-jump effective Hamiltonian  $H_{\text{eff}}$  coexisting with Poissonian spectral statistics of the Lindbladian  $\mathbb{L}$ . We show that this behavior can arise from a broad class of Lindbladians whose spectra admit a *separable structure* in Liouville space, such that the eigenvalues of  $\mathbb{L}$  are exactly constructible from those of  $H_{\text{eff}}$ , while their spectral correlations are substantially modified.

We begin by introducing this class of spectrally separable Lindbladians for a general structural level. Then, we consider a concrete realization with disordered dissipation, which completes our classification by demonstrating that Poissonian Lindbladian statistics persists despite clear signatures of chaos in the spectral properties of  $H_{\text{eff}}$ . Finally, we turn to uniform dissipation as a clean and particularly transparent realization, in which the complex Lindbladian spectrum displays Poissonian real-spacing statistics and exhibits a characteristic banded structure in Liouville space.

##### A. Spectrally separable Lindbladians

In the vectorized (Liouville-space) representation, a general Lindbladian can be written as

$$\mathbb{L} = \mathbb{H}_{\text{eff}} + \mathbb{R}, \quad (17)$$

where we introduce the Liouville-space superoperators

$$\mathbb{H}_{\text{eff}} \equiv -i(H_{\text{eff}} \otimes \mathbb{I} - \mathbb{I} \otimes H_{\text{eff}}^*), \quad \mathbb{R} \equiv \sum_i L_i \otimes L_i^*, \quad (18)$$

representing the no-jump and recycling contributions.

We consider systems in which the effective non-Hermitian Hamiltonian  $H_{\text{eff}}$  conserves a charge  $Q$  defined on the physical Hilbert space, i.e.,  $[H_{\text{eff}}, Q] = 0$ . This condition implies that the associated no-jump superoperator  $\mathbb{H}_{\text{eff}}$  preserves the total charge, so that  $[\mathbb{H}_{\text{eff}}, \mathcal{Q}] = 0$ , where  $\mathcal{Q} = Q_{\text{ket}} + Q_{\text{bra}}$

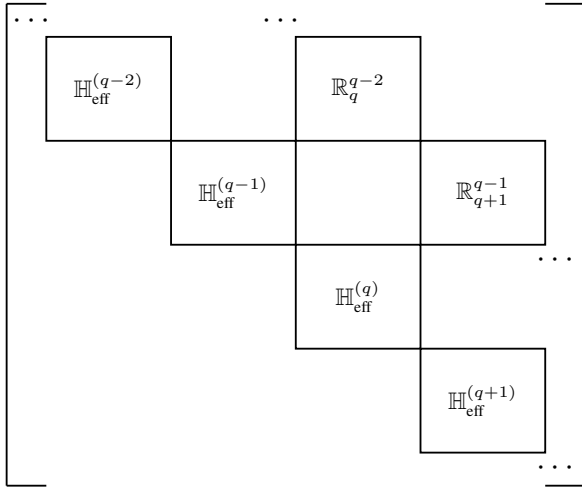


FIG. 4. Schematic block-triangular structure of  $\mathbb{L} = \mathbb{H}_{\text{eff}} + \mathbb{R}$  in a basis ordered by the total Liouville-space charge  $\mathcal{Q}$ . The no-jump superoperator  $\mathbb{H}_{\text{eff}}$  is block diagonal with blocks  $\mathbb{H}_{\text{eff}}^{(q)}$  acting within fixed- $q$  sectors. For jump operators that lower the physical charge by one unit, the recycling term  $\mathbb{R} = \sum_i L_i \otimes L_i^*$  connects only sectors  $q \rightarrow q - 2$ , yielding nonzero off-diagonal blocks  $\mathbb{R}_q^{q-2}$ . Block sizes are schematic and not drawn to scale.

labels the sum of the charges in the ket and bra spaces. As a result,  $\mathbb{H}_{\text{eff}}$  is block diagonal in a basis ordered by  $\mathcal{Q}$ .

In contrast, we further assume that the jump operators  $L_i$  act in a strictly one-sided manner on the charge sectors of  $\mathcal{Q}$ , i.e., either lowering or raising the charge. In what follows, we focus on the lowering case. If  $L_i$  lowers the charge by one unit, the recycling term  $\mathbb{R}$  lowers the total Liouville-space charge by two units. Consequently,  $\mathbb{R}$  connects only sectors labeled by the eigenvalue  $q$  of  $\mathcal{Q}$  with  $q \rightarrow q - 2$ , and therefore appears exclusively in off-diagonal blocks.

In the  $\mathcal{Q}$ -ordered basis, the full Lindbladian acquires a block-triangular structure, with diagonal blocks given by those of  $\mathbb{H}_{\text{eff}}$  (see Fig. 4), which we refer to as  $\mathbb{H}_{\text{eff}}^{(q)}$ . A direct consequence is that the eigenvalue set of  $\mathbb{L}$  is completely determined by its diagonal blocks, i.e.,

$$\text{spec}(\mathbb{L}) = \text{spec}(\mathbb{H}_{\text{eff}}) = \bigcup_q \text{spec}(\mathbb{H}_{\text{eff}}^{(q)}), \quad (19)$$

More explicitly, if  $E_\mu$  denotes an eigenvalue of the  $H_{\text{eff}}$ , the spectrum of the no-jump superoperator  $\mathbb{H}_{\text{eff}}$  is given by pairwise differences of these eigenvalues,

$$\lambda_{\mu\nu} = -i(E_\mu - E_\nu^*). \quad (20)$$

This decoupled difference structure makes explicit that the Lindbladian spectrum is constructed from two independent copies of the  $H_{\text{eff}}$  spectrum. We refer to this construction as *spectrally separable*. Related triangular structures for loss-only Lindbladians with a conserved charge have also been discussed [73–75], primarily in the context of exact spectral constructions and relaxation properties.

It is important to emphasize that this spectral separability does not mean a symmetry decomposition of the Lindbladian. Although the set of eigenvalues of  $\mathbb{L}$  is completely

determined by the diagonal blocks of  $\mathbb{H}_{\text{eff}}$ , the off-diagonal recycling terms  $\mathbb{R}$  generically mix different charge sectors at the level of eigenmodes. Consequently, spectral statistics are evaluated for the full  $\mathbb{L}$  rather than within individual diagonal blocks. Within this setting, the decoupled difference structure of the Lindbladian spectrum naturally suppresses level repulsion, and we therefore expect Poissonian spectral statistics, as demonstrated numerically below.

We now turn to concrete realizations of the spectrally separable structure discussed above. A particularly natural setting is provided by spin chains with conserved total magnetization. The coherent Hamiltonian  $H$  preserves the charge of  $\mathcal{Q} = \sum_i \sigma_i^z$ , while dissipation is implemented through local spin-lowering jump operators, as defined in Eq. (12), with site-dependent rates  $\gamma_i$ . These choices ensure that the no-jump effective Hamiltonian  $H_{\text{eff}}$  conserves the charge  $\mathcal{Q}$ , whereas the recycling term changes the corresponding Liouville-space charge in a strictly one-sided manner.

## B. Disordered dissipation realization

We first consider the case of disordered dissipation,  $L_i = \sqrt{\gamma_i} \sigma_i^-$ , where the damping rates  $\gamma_i$  are taken to be site dependent. As a concrete realization, we choose the coherent Hamiltonian  $H$  to be the interacting XXZ chain introduced in Eq. (15). Disorder is implemented by sampling the rates  $\{\gamma_i\}$  independently from a uniform distribution  $\gamma_i \in [0, \gamma]$ , where  $\gamma$  controls the disorder strength. For  $H_{\text{eff}}$ , we focus on the zero-magnetization sector ( $m_p = 0$ ) at chain length  $L = 18$ . For the Lindbladian  $\mathbb{L}$ , we consider a physical chain of length  $L = 9$  and restrict to the  $m_d = 0$  symmetry sector. Throughout, we set  $\Delta = J$ .

Fig. 5 shows the CSR distributions for the no-jump effective Hamiltonian  $H_{\text{eff}}$  [Figs. 5(a), (c)] and for the Lindbladian  $\mathbb{L}$  [Figs. 5(b), (d)] at  $\gamma = 2$  and  $\gamma = 20$ , respectively. For  $\gamma = 2$ , the CSR distribution of  $H_{\text{eff}}$  is strongly nonuniform [Fig. 5(a)], consistent with chaotic spectral correlations. Here, chaos arises from the presence of disordered dissipation, which breaks the integrable structure present under uniform damping. By contrast, the Lindbladian spectrum exhibits a nearly uniform CSR distribution [Fig. 5(b)], indicating Poissonian statistics despite the chaotic signature of  $H_{\text{eff}}$ . This behavior reflects the fact that the Lindbladian's spectral statistics are governed by the underlying spectrally separable Liouville-space structure, rather than by the detailed spectral correlations of  $H_{\text{eff}}$ .

Upon increasing the disorder strength to  $\gamma = 20$ , the CSR distribution of  $H_{\text{eff}}$  becomes much closer to a uniform disk within the system sizes accessible here [Fig. 5(c)], indicating, for this system size, strongly reduced spectral correlations and a Poisson-like regime. A similar change from chaotic to regular has been reported for the same non-Hermitian Hamiltonian in Ref. [76], where singular-value based diagnostics provide evidence for a localization-like regime at strong dissipation disorder. We emphasize that a systematic finite-size scaling would clarify the nature of this crossover/transition, but this is beyond the scope of this work. In contrast, the Lindbladian's

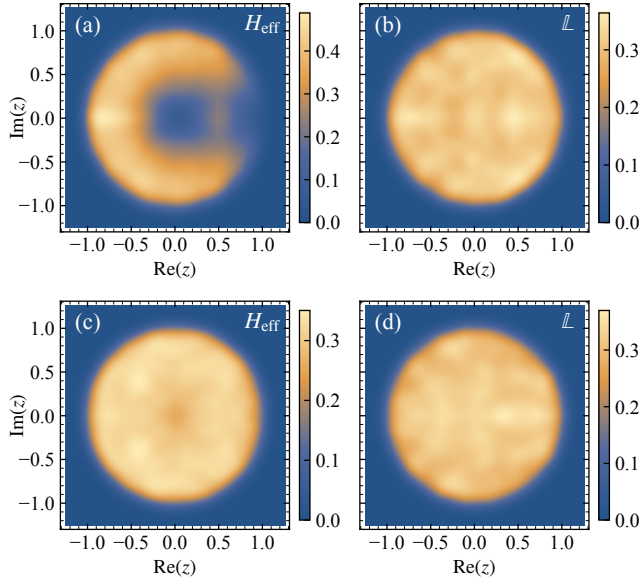


FIG. 5. Complex-spacing-ratio (CSR) distributions for the no-jump effective Hamiltonian  $H_{\text{eff}}$  and the Lindbladian  $\mathbb{L}$  in the disordered damped  $XXZ$  chain. (a) and (c) show  $H_{\text{eff}}$  at different disorder strength,  $\hbar\gamma = 2J$  and  $20J$ , respectively, while panels (b) and (d) show the corresponding results for  $\mathbb{L}$ .

CSR distribution remains essentially unchanged [Fig. 5(d)], further illustrating the robustness of Poissonian statistics for Lindbladian within the  $U(1)$ -symmetric damping family.

### C. Uniform damping and band spectral structure

To gain further insight into the consequences of spectral separability in Liouville space, we now turn to a particularly clean realization within the  $U(1)$ -symmetric damping family. In this setting, dissipation is taken to be uniform,  $L_i = \sqrt{\gamma}\sigma_i^-$ , while the coherent Hamiltonian  $H$  itself is non-integrable and exhibits chaotic spectral statistics. We illustrate this structure using a next-to-nearest-neighbor (NNN) Heisenberg  $XXZ$  chain with Hamiltonian

$$H = J \sum_{i=1}^{L-1} (\sigma_i^x \sigma_{i+1}^x + \sigma_i^y \sigma_{i+1}^y + \Delta \sigma_i^z \sigma_{i+1}^z) + J' \sum_{i=1}^{L-2} (\sigma_i^x \sigma_{i+2}^x + \sigma_i^y \sigma_{i+2}^y + \Delta' \sigma_i^z \sigma_{i+2}^z), \quad (21)$$

where  $J(J')$  denotes the nearest- (next-to-nearest-) neighbor exchange coupling, and  $\Delta(\Delta')$  the corresponding  $z$ -axis anisotropy. Dissipation is implemented via uniform damping rates  $\gamma_i \equiv \gamma$  [Eq. (12)]. We work in the zero-magnetization sector for  $H_{\text{eff}}$ . Within this sector, two additional symmetries, spin inversion ( $Z_2$ ) and spatial reflection ( $P_x$ ), are present, and we focus on the even- $Z_2$  and even- $P_x$  sector. For the Lindbladian  $\mathbb{L}$ , the magnetization difference  $\mathcal{M}_d$  is conserved, and we restrict to  $m_d = 0$  and even- $P_x$ . We set  $J' = J, \Delta =$

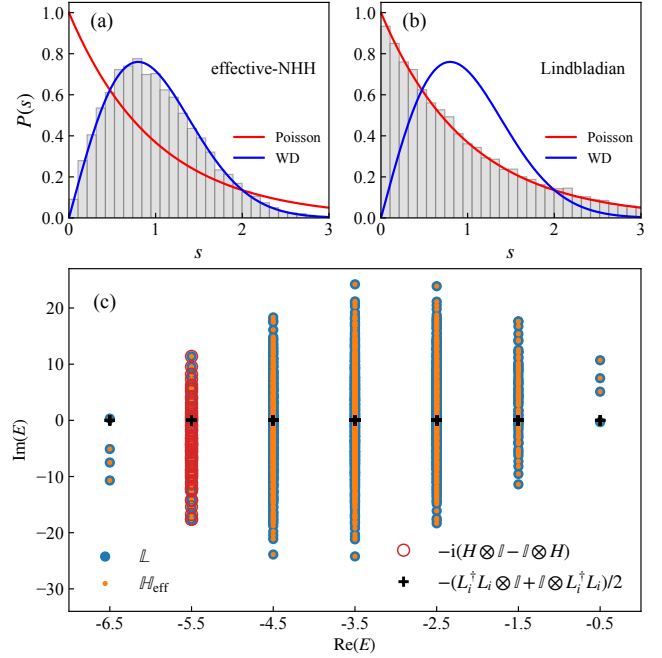


FIG. 6. Spectral diagnostics for the next-to-nearest-neighbor Heisenberg  $XXZ$  chain with uniform damping. (a), (b) Nearest-neighbor level-spacing distribution  $P(s)$  for  $H_{\text{eff}}$  and for  $\mathbb{L}$ , respectively; the red and blue curves are the Poisson and Wigner-Dyson reference distributions for real-spectrum level statistics. (c) Complex spectrum of  $\mathbb{L}$  (blue dots) and of the no-jump superoperator  $\mathbb{H}_{\text{eff}}$  (orange dots). Black crosses indicate the damping shifts from  $-(L_i^\dagger L_i \otimes \mathbb{I} + \mathbb{I} \otimes L_i^\dagger L_i)/2$ , and the red circles show the spectrum of the coherent part  $-i(H \otimes \mathbb{I} - \mathbb{I} \otimes H)$  in the ( $m_{\text{ket}} = 5, m_{\text{bra}} = 3$ ) block (with  $m_d = 2$ ).

$0.5J, \Delta' = 1.5J$ , and consider chains of length  $L = 10$  for  $\mathbb{L}$  and  $L = 20$  for  $H_{\text{eff}}$  with damping strength  $\hbar\gamma = J$ .

Although both  $H_{\text{eff}}$  and the Lindbladian  $\mathbb{L}$  are non-Hermitian operators, their level-spacing statistics are well described by the familiar distributions of Hermitian systems. As shown in Fig. 6(a), the level-spacing distribution  $P(s)$  of  $H_{\text{eff}}$  agrees well with the Wigner-Dyson form,  $P(s) = (\pi s/2) \exp(-\pi s^2/4)$  [42, 77], indicating statistics consistent with the Gaussian orthogonal ensemble (GOE). This behavior follows directly from the structure of  $H_{\text{eff}}$ . For uniform jumps, the non-Hermitian contribution to  $H_{\text{eff}}$  is proportional to  $\sum_i L_i^\dagger L_i$ , which reduces to  $\gamma(M + L)/2$ , where  $M = \sum_i \sigma_i^z$  is the conserved magnetization and  $L$  is the chain length. It therefore contributes only a constant within each fixed-magnetization sector. Accordingly, the spectral statistics of  $H_{\text{eff}}$  coincide with those of the underlying nonintegrable NNN Heisenberg Hamiltonian, displaying GOE statistics in the relevant symmetry sector.

In contrast, the Lindbladian spacing distribution  $P(s)$  shown in Fig. 6(b) is well described by the Poisson distribution,  $P(s) = e^{-s}$  [78–80], exhibiting the uncorrelated spacing behavior familiar from integrable Hermitian systems, despite the fact that  $\mathbb{L}$  possesses a generically complex spectrum.

The essential ingredient for understanding this behavior is

that the coherent Hamiltonian  $H$  commutes with the non-Hermitian contribution,

$$[H, \sum_i L_i^\dagger L_i] = 0, \quad (22)$$

which implies that the two operators can be simultaneously diagonalized. Since the no-jump superoperator can be written as  $\mathbb{H}_{\text{eff}} = -i(H \otimes \mathbb{I} - \mathbb{I} \otimes H) - \frac{\gamma}{4}(\mathcal{M}_p + 2L)$ , this simultaneous diagonalizability lifts directly to Liouville space. As a consequence, the eigenvalues of  $\mathbb{H}_{\text{eff}}$  take the simple form

$$\lambda_{\alpha\beta}^{(m_p)} = -i(E_\alpha - E_\beta) - \frac{\gamma}{4}(m_p + 2L), \quad (23)$$

where  $E_\alpha$  and  $E_\beta$  are eigenenergies of  $H$ , and  $m_p$  denotes the total magnetization of the corresponding Liouville state. We note that, as discussed in Sec. IV A, these eigenvalues coincide with those of the full Lindbladian  $\mathbb{L}$ . The coherent part therefore generates purely imaginary eigenvalues given by energy differences, while the damping term contributes only a constant real shift controlled by  $m_p$ .

Since the Lindbladian  $\mathbb{L}$  conserves only the magnetization difference  $\mathcal{M}_d$ , its spectrum must be analyzed within fixed  $m_d$  sectors. Within a given  $m_d$  sector, the total magnetization  $m_p$  is not conserved and can take only a discrete set of allowed values. As a result, the real parts of the eigenvalues,  $-\frac{\gamma}{4}(m_p + 2L)$ , form a discrete and equally spaced set, giving rise to a characteristic banded structure in the complex plane. Within each band, the eigenvalues originate from energy differences of the underlying coherent Hamiltonian and are expected to be only weakly correlated. Nearest neighbors in the complex plane are therefore predominantly drawn from within the same band, leading to effectively uncorrelated real-part spacings and hence Poisson statistics.

Fig. 6(c) provides a direct numerical confirmation of this picture. The eigenvalues of the full Lindbladian  $\mathbb{L}$  (blue dots) coincide with those of  $\mathbb{H}_{\text{eff}}$  (orange dots), consistent with the block-triangular structure discussed in Sec. IV A. The red circles and black crosses correspond to the two commuting contributions  $-i(H \otimes \mathbb{I} - \mathbb{I} \otimes H)$  and  $-(\gamma/4)(\mathcal{M}_p + 2L)$  appearing in  $\mathbb{H}_{\text{eff}}$ , respectively, illustrating how the two terms combine additively in the spectrum. Because  $m_p$  takes discrete values within a fixed- $m_d$  sector, the real shifts form an equally spaced set, and each vertical band is obtained by adding the imaginary energy-difference spectrum to one such shift. This construction explains the band centers and their vertical extent, and it also rationalizes why the nearest-neighbor spacings are dominated by intra-band pairs.

In the uniform-dissipation setting considered here, the analysis above makes explicit how the separable structure of Liouville space organizes the spectrum. The coherent Hamiltonian, the non-Hermitian damping terms, and the recycling processes contribute in a clearly distinguishable manner, giving rise to a rigid banded structure and Poissonian real-spacing statistics, despite the spectrum being genuinely complex. In this way, the uniform-dissipation case provides a particularly transparent illustration of Poissonian statistics in Lindbladians arising from spectral separability. For completeness, we note that a similar banded (or stripe-like) structure has also

been reported in Ref. [81] for driven-dissipative hard-core bosons with both local pump and loss. In that case, however, the bands arise only perturbatively in the weak-dissipation regime, providing a complementary perspective on how deviations from strictly one-sided dissipation (e.g. only losses or pumping) restore chaotic non-Hermitian spectral behavior.

## V. SUMMARY

In this work, we investigate how spectral statistics of Lindbladians  $\mathbb{L}$  relate to those of their associated no-jump effective non-Hermitian Hamiltonians  $H_{\text{eff}}$ . Using a ladder representation and symmetry-resolved complex-spectrum diagnostics, we systematically characterize integrable versus chaotic spectral statistics of both  $\mathbb{L}$  and  $H_{\text{eff}}$ . Notably, we realize all combinations of chaotic and regular effective Hamiltonian and Lindbladians in paradigmatic dissipative spin chains, while also uncovering a broad class of structurally separable Lindbladians whose complex spectra exhibit robust Poisson statistics.

We first show that dissipation drives both  $\mathbb{L}$  and  $H_{\text{eff}}$  into a chaotic regime with closely matching spectral statistics in the locally damped transverse-field Ising chain. We then explore whether integrable spectral statistics of  $H_{\text{eff}}$  are necessarily inherited by the full Lindbladian  $\mathbb{L}$ . Comparing an  $XXZ$  chain with a transverse-field Ising chain, we find that the inheritance is highly sensitive to the underlying integrable structure. Specifically, with identical dephasing jump operators, the interacting  $XXZ$  model shows chaotic Lindbladian statistics, whereas the free-fermionic transverse-field Ising chain retains integrable statistics for both  $\mathbb{L}$  and  $H_{\text{eff}}$ .

Finally, we identify a broad structural family of Lindbladians whose Liouville-space spectra are spectrally separable and can be constructed exactly from the spectrum of the associated  $H_{\text{eff}}$ . Within this family, the Lindbladian generically exhibits Poissonian spectral statistics, even when  $H_{\text{eff}}$  displays chaotic correlations or undergoes a disorder-driven change toward Poisson-like behavior. In the special case of uniform damping, we further uncover a novel phenomenology in which the level statistics resemble those of a real-spectrum Poisson ensemble, despite the Lindbladian possessing a genuinely complex spectrum. This illustrates how structural constraints in Liouville space can suppress level repulsion and provides a realization of the chaotic-to-integrable scenario in our classification.

Our results highlight that recycling processes, symmetry constraints, and the organization of Liouville space play a decisive role in shaping spectral universality in open many-body systems. Several open directions naturally follow from our work. First, it remains to be understood which integrable structures can retain Poissonian statistics once recycling-induced couplings are included. A second direction is to explore how the spectral separability extends to more general dissipative channels, and to clarify its dynamical implications, including relaxation [82], thermalization [23–25] and localization [19–22] behavior. More broadly, it would be interesting to connect these questions to broader non-Hermitian

and driven open systems, such as models with gain and loss competition [55, 83], Liouvillian exceptional points [84], or Floquet Lindbladians [85].

## VI. ACKNOWLEDGMENTS

We warmly thank Lucas Sà for helpful advice and correspondence. D.W. and D.P. acknowledge support from the Singapore Ministry of Education grant MOE-T2EP50123-0017, and from the Centre for Quantum Technologies grant CQT\_SUTD\_2025\_01. H.Z. and GF.Z. acknowledge support from the National Natural Science Foundation of China (Grant No. 12474353).

- 
- [1] H.-P. Breuer and F. Petruccione, *The Theory of Open Quantum Systems* (Oxford University Press, Oxford, 2007).
- [2] U. Weiss, *Quantum Dissipative Systems* (World Scientific, Singapore, 2000).
- [3] A. Rivas and S. F. Huelga, *Open Quantum Systems: An Introduction* (Springer, Berlin, Heidelberg, 2012).
- [4] V. Gorini, A. Kossakowski, and E. C. G. Sudarshan, Completely positive dynamical semigroups of N-level systems, *J. Math. Phys.* **17**, 821 (1976).
- [5] G. Lindblad, On the generators of quantum dynamical semigroups, *Commun. Math. Phys.* **48**, 119 (1976).
- [6] R. Alicki and K. Lendi, *Quantum Dynamical Semigroups and Applications* (Springer, Berlin, 1987).
- [7] G. T. Landi, D. Poletti, and G. Schaller, Nonequilibrium boundary-driven quantum systems: Models, methods, and properties, *Rev. Mod. Phys.* **94**, 045006 (2022).
- [8] T. Prosen, Third quantization: a general method to solve master equations for quadratic open Fermi systems, *New Journal of Physics* **10**, 043026 (2008).
- [9] D. Karevski, V. Popkov, and G. M. Schütz, Exact matrix product solution for the boundary-driven lindblad  $xxz$  chain, *Phys. Rev. Lett.* **110**, 047201 (2013).
- [10] M. V. Medvedyeva, F. H. L. Essler, and T. Prosen, Exact bethe ansatz spectrum of a tight-binding chain with dephasing noise, *Phys. Rev. Lett.* **117**, 137202 (2016).
- [11] L. Banchi, D. Burgarth, and M. J. Kastoryano, Driven quantum dynamics: Will it blend?, *Phys. Rev. X* **7**, 041015 (2017).
- [12] D. A. Rowlands and A. Lamacraft, Noisy spins and the richardson-gaudin model, *Phys. Rev. Lett.* **120**, 090401 (2018).
- [13] P. Ribeiro and T. Prosen, Integrable quantum dynamics of open collective spin models, *Phys. Rev. Lett.* **122**, 010401 (2019).
- [14] L. Sá, P. Ribeiro, and T. Prosen, Spectral and steady-state properties of random Liouvillians, *Journal of Physics A Mathematical General* **53**, 305303 (2020).
- [15] S. Denisov, T. Lapyteva, W. Tarnowski, D. Chruściński, and K. Życzkowski, Universal spectra of random lindblad operators, *Phys. Rev. Lett.* **123**, 140403 (2019).
- [16] T. Can, V. Oganessian, D. Orgad, and S. Gopalakrishnan, Spectral gaps and midgap states in random quantum master equations, *Phys. Rev. Lett.* **123**, 234103 (2019).
- [17] T. Can, Random Lindblad dynamics, *Journal of Physics A Mathematical General* **52**, 485302 (2019).
- [18] R. Hamazaki, M. Nakagawa, T. Haga, and M. Ueda, Lindbladian many-body localization (2022), [arXiv:2206.02984](https://arxiv.org/abs/2206.02984) [cond-mat.dis-nn].
- [19] R. Hamazaki, K. Kawabata, and M. Ueda, Non-hermitian many-body localization, *Phys. Rev. Lett.* **123**, 090603 (2019).
- [20] X. Xu, C. Guo, and D. Poletti, Interplay of interaction and disorder in the steady state of an open quantum system, *Phys. Rev. B* **97**, 140201 (2018).
- [21] X. Xu and D. Poletti, Localization-delocalization effects of a delocalizing dissipation on disordered  $xxz$  spin chains, *Chaos* **31**, 033133 (2021).
- [22] I. Vakulchyk, I. Yusipov, M. Ivanchenko, S. Flach, and S. Denisov, Signatures of many-body localization in steady states of open quantum systems, *Phys. Rev. B* **98**, 020202 (2018).
- [23] S. Moudgalya, T. Devakul, D. P. Arovas, and S. L. Sondhi, Extension of the eigenstate thermalization hypothesis to nonequilibrium steady states, *Phys. Rev. B* **100**, 045112 (2019).
- [24] S. Singha Roy, S. Bandyopadhyay, R. Costa de Almeida, and P. Hauke, Unveiling eigenstate thermalization for non-hermitian systems, *Phys. Rev. Lett.* **134**, 180405 (2025).
- [25] G. Almeida, P. Ribeiro, M. Haque, and L. Sá, Universality, robustness, and limits of the eigenstate thermalization hypothesis in open quantum systems, *Phys. Rev. E* **113**, L012101 (2026).
- [26] J. Dalibard, Y. Castin, and K. Mølmer, Wave-function approach to dissipative processes in quantum optics, *Phys. Rev. Lett.* **68**, 580 (1992).
- [27] R. Dum, P. Zoller, and H. Ritsch, Monte carlo simulation of the atomic master equation for spontaneous emission, *Phys. Rev. A* **45**, 4879 (1992).
- [28] R. Dum, A. S. Parkins, P. Zoller, and C. W. Gardiner, Monte carlo simulation of master equations in quantum optics for vacuum, thermal, and squeezed reservoirs, *Phys. Rev. A* **46**, 4382 (1992).
- [29] K. Mølmer, Y. Castin, and J. Dalibard, Monte carlo wave-function method in quantum optics, *J. Opt. Soc. Am. B* **10**, 524 (1993).
- [30] M. B. Plenio and P. L. Knight, The quantum-jump approach to dissipative dynamics in quantum optics, *Rev. Mod. Phys.* **70**, 101 (1998).
- [31] A. J. Daley, Quantum trajectories and open many-body quantum systems, *Advances in Physics* **63**, 77 (2014).
- [32] T. E. Lee and C.-K. Chan, Heralded magnetism in non-hermitian atomic systems, *Phys. Rev. X* **4**, 041001 (2014).
- [33] K. Yamamoto, M. Nakagawa, K. Adachi, K. Takasan, M. Ueda, and N. Kawakami, Theory of non-hermitian fermionic superfluidity with a complex-valued interaction, *Phys. Rev. Lett.* **123**, 123601 (2019).
- [34] K. Yang, S. C. Morampudi, and E. J. Bergholtz, Exceptional spin liquids from couplings to the environment, *Phys. Rev. Lett.* **126**, 077201 (2021).
- [35] M. L. Mehta, *Random Matrices* (Academic Press, New York, 2004).
- [36] O. Bohigas, M. J. Giannoni, and C. Schmit, Characterization of Chaotic Quantum Spectra and Universality of Level Fluctuation Laws, *Phys. Rev. Lett.* **52**, 1 (1984).

- [37] J. M. Deutsch, Quantum statistical mechanics in a closed system, *Phys. Rev. A* **43**, 2046 (1991).
- [38] M. Srednicki, Chaos and quantum thermalization, *Phys. Rev. E* **50**, 888 (1994).
- [39] F. Haake, *Quantum Signatures of Chaos* (Springer, Berlin, 2010).
- [40] G. Casati, F. Valz-Gris, and I. Guarneri, On the connection between quantization of nonintegrable systems and statistical theory of spectra, *Nuovo Cimento* **28**, 279 (1980).
- [41] O. Bohigas, M. J. Giannoni, and C. Schmit, Characterization of chaotic quantum spectra and universality of level fluctuation laws, *Phys. Rev. Lett.* **52**, 1 (1984).
- [42] T. Guhr, A. Müller-Groeling, and H. A. Weidenmüller, Random-matrix theories in quantum physics: common concepts, *Physics Reports* **299**, 189 (1998).
- [43] R. Grobe, F. Haake, and H.-J. Sommers, Quantum distinction of regular and chaotic dissipative motion, *Phys. Rev. Lett.* **61**, 1899 (1988).
- [44] G. Akemann, M. Kieburg, A. Mielke, and T. Prosen, Universal signature from integrability to chaos in dissipative open quantum systems, *Phys. Rev. Lett.* **123**, 254101 (2019).
- [45] L. Sá, P. Ribeiro, and T. Prosen, Complex spacing ratios: A signature of dissipative quantum chaos, *Physical Review X* **10**, 021019 (2020).
- [46] R. Hamazaki, K. Kawabata, N. Kura, and M. Ueda, Universality classes of non-Hermitian random matrices, *Phys. Rev. Res.* **2**, 023286 (2020).
- [47] K. Kawabata, Z. Xiao, T. Ohtsuki, and R. Shindou, Singular-value statistics of non-hermitian random matrices and open quantum systems, *PRX Quantum* **4**, 040312 (2023).
- [48] K. Wang, F. Piazza, and D. J. Luitz, Hierarchy of relaxation timescales in local random liouvillians, *Phys. Rev. Lett.* **124**, 100604 (2020).
- [49] J. Li, T. Prosen, and A. Chan, Spectral statistics of non-hermitian matrices and dissipative quantum chaos, *Phys. Rev. Lett.* **127**, 170602 (2021).
- [50] A. Rubio-García, R. Molina, and J. Dukelsky, From integrability to chaos in quantum Liouvillians, *SciPost Physics Core* **5**, 026 (2022).
- [51] J. Cornelius, Z. Xu, A. Saxena, A. Chenu, and A. del Campo, Spectral filtering induced by non-hermitian evolution with balanced gain and loss: Enhancing quantum chaos, *Phys. Rev. Lett.* **128**, 190402 (2022).
- [52] A. M. García-García, L. Sá, and J. J. M. Verbaarschot, Symmetry classification and universality in non-hermitian many-body quantum chaos by the sachdev-ye-kitaev model, *Phys. Rev. X* **12**, 021040 (2022).
- [53] G. Cipolloni and J. Kudler-Flam, Entanglement entropy of non-hermitian eigenstates and the ginibre ensemble, *Phys. Rev. Lett.* **130**, 010401 (2023).
- [54] A. M. García-García, L. Sá, and J. J. M. Verbaarschot, Universality and its limits in non-hermitian many-body quantum chaos using the sachdev-ye-kitaev model, *Phys. Rev. D* **107**, 066007 (2023).
- [55] K. Kawabata, K. Shiozaki, M. Ueda, and M. Sato, Symmetry and topology in non-hermitian physics, *Phys. Rev. X* **9**, 041015 (2019).
- [56] H. Zhou and J. Y. Lee, Periodic table for topological bands with non-hermitian symmetries, *Phys. Rev. B* **99**, 235112 (2019).
- [57] S. Lieu, M. McGinley, and N. R. Cooper, Tenfold way for quadratic lindbladlans, *Phys. Rev. Lett.* **124**, 040401 (2020).
- [58] L. Sá, P. Ribeiro, and T. Prosen, Symmetry classification of many-body lindbladlans: Tenfold way and beyond, *Phys. Rev. X* **13**, 031019 (2023).
- [59] K. Kawabata, A. Kulkarni, J. Li, T. Numasawa, and S. Ryu, Symmetry of open quantum systems: Classification of dissipative quantum chaos, *PRX Quantum* **4**, 030328 (2023).
- [60] K. H. Lee, V. Balachandran, C. Guo, and D. Poletti, Transport and spectral properties of the  $xx + xxz$  diode and stability to dephasing, *Phys. Rev. E* **105**, 024120 (2022).
- [61] B. Buča and T. Prosen, A note on symmetry reductions of the Lindblad equation: transport in constrained open spin chains, *New Journal of Physics* **14**, 073007 (2012).
- [62] Here, by  $e^{t\mathcal{L}}(\rho)$  we mean the evolution of the density matrix  $\rho$  for a time  $t$  using Eq. (1).
- [63] J. Ginibre, Statistical ensembles of complex, quaternion, and real matrices, *Journal of Mathematical Physics* **6**, 440 (1965).
- [64] H. Markum, R. Pullirsch, and T. Wettig, Non-Hermitian Random Matrix Theory and Lattice QCD with Chemical Potential, *Phys. Rev. Lett.* **83**, 484 (1999).
- [65] J. Feinberg and A. Zee, Non-hermitian random matrix theory: Method of hermitian reduction, *Nuclear Physics B* **504**, 579 (1997).
- [66] V. Oganesyan and D. A. Huse, Localization of interacting fermions at high temperature, *Phys. Rev. B* **75**, 155111 (2007).
- [67] Y. Y. Atas, E. Bogomolny, O. Giraud, and G. Roux, Distribution of the Ratio of Consecutive Level Spacings in Random Matrix Ensembles, *Phys. Rev. Lett.* **110**, 084101 (2013).
- [68] M. Baggioli, K.-B. Huh, H.-S. Jeong, X. Jiang, K.-Y. Kim, and J. F. Pedraza, Singular value decomposition and its blind spot for quantum chaos in non-hermitian sachdev-ye-kitaev models, *Phys. Rev. D* **111**, L101904 (2025).
- [69] H. You, J. Liu, Y. Zhang, and Z. Xu, Limitations of SVD-Based Diagnostics for Non-Hermitian Many-Body Localization with Time-Reversal Symmetry, *arXiv e-prints*, arXiv:2602.07349 (2026).
- [70] P. J. Forrester, *Log-Gases and Random Matrices* (Princeton University Press, Princeton, NJ, 2010).
- [71] D. Chafaï and G. Ferré, Simulating Coulomb and Log-Gases with Hybrid Monte Carlo Algorithms, *J. Stat. Phys.* **174**, 692 (2019).
- [72] As in many finite-size spectral diagnostics, convergence to the random-matrix class values typically improves with increasing matrix dimension (Hilbert-space for  $H_{\text{eff}}$  and Liouville-space for  $\mathbb{L}$ ); correspondingly, the crossover in  $\langle r \rangle$  may occur at smaller  $\gamma$  for larger system sizes.
- [73] J. M. Torres, Closed-form solution of lindblad master equations without gain, *Phys. Rev. A* **89**, 052133 (2014).
- [74] B. Buča, C. Booker, M. Medenjak, and D. Jaksch, Bethe ansatz approach for dissipation: exact solutions of quantum many-body dynamics under loss, *New J. Phys.* **22**, 123040 (2020).
- [75] M. Nakagawa, N. Kawakami, and M. Ueda, Exact liouvilian spectrum of a one-dimensional dissipative hubbard model, *Phys. Rev. Lett.* **126**, 110404 (2021).
- [76] F. Roccati, F. Balducci, R. Shir, and A. Chenu, Diagnosing non-hermitian many-body localization and quantum chaos via singular value decomposition, *Phys. Rev. B* **109**, L140201 (2024).
- [77] M. V. Berry and M. Tabor, Level Clustering in the Regular Spectrum, *Proc. R. Soc. A* **356**, 375 (1977).
- [78] A. Pandey and R. Ramaswamy, Level spacings for harmonic-oscillator systems, *Phys. Rev. A* **43**, 4237 (1991).
- [79] P. R. Zangara, A. D. Dente, E. J. Torres-Herrera, H. M. Pastawski, A. Iucci, and L. F. Santos, Time fluctuations in isolated quantum systems of interacting particles, *Phys. Rev. E* **88**, 032913 (2013).
- [80] M. A. Garcia-March, S. van Frank, M. Bonneau, J. Schmiedmayer, M. Lewenstein, and L. F. Santos, Relaxation, chaos, and thermalization in a three-mode model of a Bose-Einstein con-

- densate, *New Journal of Physics* **20**, 113039 (2018).
- [81] M. Zündel, Nonintegrability of driven-dissipative one-dimensional hard-core bosons, *Phys. Rev. A* **112**, 013303 (2025).
- [82] M. Žnidarič, Relaxation times of dissipative many-body quantum systems, *Phys. Rev. E* **92**, 042143 (2015).
- [83] C. M. Bender, Making sense of non-Hermitian Hamiltonians, *Reports on Progress in Physics* **70**, 947 (2007).
- [84] F. Minganti, A. Miranowicz, R. W. Chhajlany, and F. Nori, Quantum exceptional points of non-hermitian hamiltonians and liouvillians: The effects of quantum jumps, *Phys. Rev. A* **100**, 062131 (2019).
- [85] A. Lazarides, A. Das, and R. Moessner, Equilibrium states of generic quantum systems subject to periodic driving, *Phys. Rev. E* **90**, 012110 (2014).